대한기계학회 2000년도 춘계학술대회논문집 B pp. 514~519 KSME 00S240

EXPERIMENTAL AND COMPUTATIONAL STUDIES ON HYSTERISYS PHENOMENON OF SUPERSONIC COANDA WALL JETS

Heuydong Kim*, Ohsik Kweon** and Toshiaki Setoguchi***

Key Words : Compressible Flow, Supersonic Flow, Shock Wave, Coanda Jet, Separation

Abstract

Recently a considerable interest is being concentrated on industrial applications of supersonic Coanda wall jets, but the flow physics are not still understood well. It is of practical importance to evaluate the effectiveness of supersonic Coanda wall jet devices for such industrial purposes. In the present work, experiments and computations were performed to get a better understanding of the supersonic Coanda jet physics. The experiments were made using a small blow-down wind tunnel. The operating pressure ratio and the Coanda surface configuration were changed to investigate their influences on the wall jet flows. Two-dimensional Navier-Stokes computations were performed using a TVD finite volume scheme to effectively capture the important wave structures of supersonic Coanda jet flows. Both experimental and computational results showed several important hysterical features of the supersonic Coanda wall jets; the attachment and detachment of supersonic Coanda jet were strongly dependent on the change processes of the operating pressure ratio and the detailed flow configuration.

1. Introduction

The Coanda effect is the tendency for a fluid jet to attach itself to an adjacent surface and follow its contour without causing an appreciable flow separation[1,2]. The jet is pulled onto the surface by the low pressure region which develops as entrainment pumps fluid from the region between the jet and the surface. Then the jet is held to the wall surface by the resulting radial pressure gradient, which balances the inertial resistance of the jet to turning. The Coanda effect has long been applied to improve aerodynamic characteristics, such as the drag/lift ratio of flight body, the engine exhaust plume thrust vectoring, and the aerofoil/wing circulation control[3,4,5]. During the energy crisis of the seventies, the Coanda jet was applied to reduce vehicle drag and led to drag reductions of as much as about 30% for a trailer configuration. Recently a variety of industrial applications are exploiting another characteristics of the Coanda jets, mainly the enhanced turbulence levels and entrainment compared with conventional jet flows.

Various industrial burners and combustors are based upon this principle[6,7]. If the curvature of the Coanda surface is too great or the operating pressure too high, the jet flow will break away completely from the surface.

* Dept. of Mechanical Eng, Andong Univ.
** Graduate School of Mechanical Eng, Andong Univ.
*** Dept.of Mechanical Eng,Saga Univ, Japan

This could have catastrophic consequences for a burner or combustor. Detailed understanding of the Coanda jet flow is essential to refine the design to maximize the enhanced entrainment in these applications. According to the previous work[8,9], it is known that an Coanda wall jet has three distinguishing characteristics : inviscid centrifugal effect of a fluid to remain attached to a curved surfaces, viscous entrainment effect of ambient fluid to place near a surface to attach itself to the surface, and longitudinal curvature effect to cause increased entrainment and jet growth. However these findings are rather confined to the incompressible flow regime, in which the ratio of the supply total pressure of the jet to the ambient pressure was relatively small.

Compared with a large number of the work on the incompressible Coanda jet, only a few work has been made to understand the flow physics of supersonic Coanda wall jet and to develop a suitable numerical prediction method. This is not surprising because the supersonic Coanda wall jet is subject to very complicated flow phenomena such as the shock/boundary layer interaction involving a multiple of shocks embedded inside the jet flow. The supersonic Coanda jet flow in the compressible regime deserves greater attention[12] because of its large potential benefit in engineering applications.

Recently renewed interest is concentrated on the purpose of making the wall jet flow attach further to a curved surface, resulting in augmentation of a life force[10,11]. In this case, the jet flow attachment and/or detachment from the curve surface is of practical importance. As

mentioned above, the detailed configuration of the jet exhaust can have a significant influence on the jet flow detachment : Some recent work investigated the effect of the geometry of the exhaust nozzle on the jet flow field and the resulting jet detachment could be delayed considerably by employing a convergent-divergent nozzle.

The present study was performed to get a better understanding of the supersonic Coanda wall jet flow. An experiment was made using a small blow-down wind tunnel (see Fig.1). The operating pressure ratio of the supersonic Coanda wall jet was varied to obtain moderately underexpanded supersonic jets at the exit of a convergent nozzle. The radius of curvature of the Coanda surface and the height of the exhaust nozzle throat were also changed to investigate their influence on the jet flow field. Static wall pressures along the Coanda wall surface were measured to characterize the jet flow. A schlieren optical system provided a qualitative information to determine the attachment and detachments of the Coanda wall.

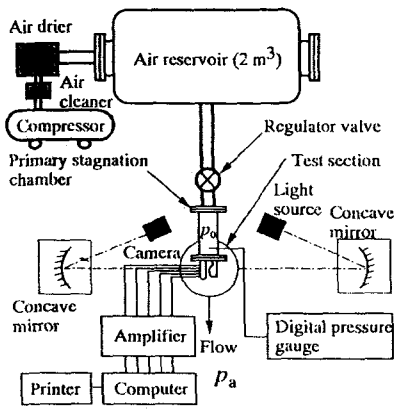

Fig.1 Schematic diagram of experimental apparatus

Two-dimensional, Navier-Stokes equations were solved to simulate the corresponding jet flows. Typical two-equation turbulence models were employed to close the governing equations, which were discretized spatially using a second-order Harten-Yee type Total Variation Diminishing(TVD) finite volume scheme on a fine structured computational grid (see Fig.3).

A third-order three stage Runge-Kutta methods were used to integrate the time derivatives in the governing equations. The computational results were compared with experiments. The effects of the radius of curvature of the Coanda surface and jet operating pressure ratio on the jet flow were discussed. Depending on the height of the exhaust nozzle, the radius of curvature of the Coanda surface, and the jet operating pressure ratio, three different flows were found : a fully attached flow without separation bubble, an attached flow with an appreciable separation bubble, and a fully detached flow. In particular, the attachment and detachments of the jet were closely associated with the process of variation of the jet operating pressure ratio.

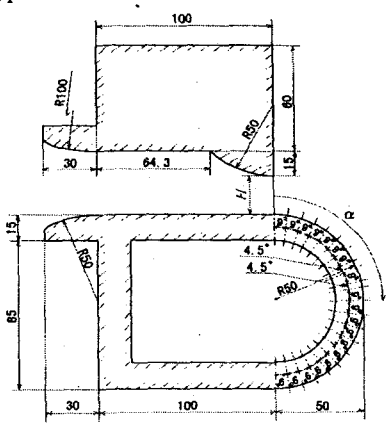

Fig.2 Details of nozzle and Coanda surface

2. Experimental Procedures

The schematic diagram of the experimental apparatus is shown in Fig.1. A wind tunnel consisted of a high pressure tank (2 m^3), a stagnation chamber and a test section. Figure 2 shows the details of nozzle and the Coanda surface having a radius of curvature of R = 50㎜. A converging nozzle (half nozzle) with a radius of curvature of 50㎜, that has a minimum height (H = 5㎜ ~ 15 ㎜) at nozzle exit, was installed between acrylic plates with a width of 50㎜.

In this apparatus, a supersonic steady flow lasting about 20 seconds was obtained in the test section. During this period, static pressures could be obtained along the Coanda wall surface. A schlieren optical system was employed for the visualization of the flow. The ratio of stagnation pressure p_0 in the reservoir to atmospheric pressure p_a can be changed from 1.1 to 5.9. The static pressures signals were measured by a scani-valve system, which was digitized with a time interval $\triangle t = 0.02$ msec (sampling frequency = 50kHz).

3. Computation

3.1 Governing Equations

In the present computation, it is assumed that the flow field has the fixed specific heats and gas constant. The governing equations under this consideration are unsteady two-dimensional compressible Navier-Stokes equations written in the Cartesian coordinate system (x, y). The governing equations, omitting the superscript*, can be written as

$$\frac{\partial Q}{\partial t}+\frac{\partial E}{\partial x}+\frac{\partial F}{\partial y}=\frac{1}{\mathrm{Re}_0}\left(\frac{\partial R}{\partial x}+\frac{\partial S}{\partial y}\right)+H \qquad (1)$$

$$Q=\begin{bmatrix}\rho\\ \rho u\\ \rho v\\ E_t\\ \rho k\\ \rho\varepsilon\end{bmatrix},E=\begin{bmatrix}\rho u\\ \rho u^2+p\\ \rho uv\\ u(E_t+p)\\ \rho ku\\ \rho\varepsilon u\end{bmatrix},F=\begin{bmatrix}\rho v\\ \rho uv\\ \rho v^2+p\\ v(E_t+p)\\ \rho kv\\ \rho\varepsilon v\end{bmatrix} \quad (2)$$

$$R=\begin{bmatrix}0\\ \tau_{xx}\\ \tau_{xy}\\ \alpha\\ \left(\mu_l+\frac{\mu_t}{\sigma_k}\right)\frac{\partial k}{\partial x}\\ \left(\mu_l+\frac{\mu_t}{\sigma_\varepsilon}\right)\frac{\partial \varepsilon}{\partial x}\end{bmatrix},S=\begin{bmatrix}0\\ \tau_{yx}\\ \tau_{yy}\\ \beta\\ \left(\mu_l+\frac{\mu_t}{\sigma_k}\right)\frac{\partial k}{\partial y}\\ \left(\mu_l+\frac{\mu_t}{\sigma_\varepsilon}\right)\frac{\partial \varepsilon}{\partial y}\end{bmatrix},H=\begin{bmatrix}0\\ 0\\ 0\\ 0\\ w\\ l\end{bmatrix} \quad (3)$$

where

$$E_t=\frac{p}{\gamma-1}+\frac{1}{2}\rho(u^2+v^2) \quad (4)$$

$$p=\rho RT \quad (5)$$

$$\alpha=u\tau_{xx}+v\tau_{yx}+\frac{\mu}{(\gamma-1)\mathrm{Pr}}\frac{\partial T}{\partial x} \quad (6)$$

$$\beta=u\tau_{xy}+v\tau_{yy}+\frac{\mu}{(\gamma-1)\mathrm{Pr}}\frac{\partial T}{\partial y} \quad (7)$$

$$w=P-\rho\varepsilon-2\left(\frac{1}{\mathrm{Re}_0}\right)\mu_l\frac{k}{y_n^2} \quad (8)$$

$$l=C_1f_1P\frac{\varepsilon}{k}-C_2f_2\frac{\varepsilon^2}{k}-2\left(\frac{1}{\mathrm{Re}_0}\right)\left(\frac{\varepsilon}{y_n^2}\right)f_3\mu_l \quad (9)$$

$$P=\left(\frac{1}{\mathrm{Re}_0}\right)\mu_t[2(u_x^2+v_y^2)+(u_y+v_x)^2 -\frac{2}{3}(u_x+u_y)^2]-\frac{2}{3}\rho k(u_x+v_y) \quad (10)$$

$$\mu_t=C_\mu f_\mu\left(\frac{\rho k^2}{\varepsilon}\right)\mathrm{Re}_0 \quad (11)$$

where, τ_{xx}, τ_{xy}, τ_{yx} and τ_{yy} are components of viscous shear stress. Three different turbulence models were used to close the governing equations.

Harten-Yee type 2nd-order upwind TVD scheme was employed in the present calculation, and Rizzi-Eriksson's third-order three stage Runge-Kutta scheme was employed for time-step scheme.

3.2 Initial and Boundary Conditions

Combinations of the Coanda surface with the radii of R = 30, 40, 50 and 60mm and the nozzle exit with the heights of H = 5, 10 and 15mm are used in the present experiments. p_0/p_a could be changed from 1.1 to 5.9. The operating pressure ration, computational grid is shown in Fig.3. The grids contain 101 divisions in ξ-direction and 101 divisions in η-direction. The minimum length is $\triangle\eta_{min} < 0.1/\mathrm{Re}_0^{0.5}$ at the near wall of solid boundaries.

Mach number is fixed by 1.0 at the nozzle exit. At the initial state of computations, atmosphere pressure and velocity in the region except the nozzle exit are set at p_a = 101.3kPa and 0, respectively. Total temperature T_0, turbulent kinetic energy k and turbulent energy dissipation rate ε are set at 293.15K, 1.5 $(0.02v_\infty)^2$ and $\varepsilon=k^{1.5}/0.01$, respectively. Here v_∞ is main flow velocity. Non-slip velocity is on the nozzle wall. Considering that flux issuing from wall is 0, other physical quantities are calculated using flux vectors on the cell boundary surface. Exit boundaries are constrained with outflow boundary condition.

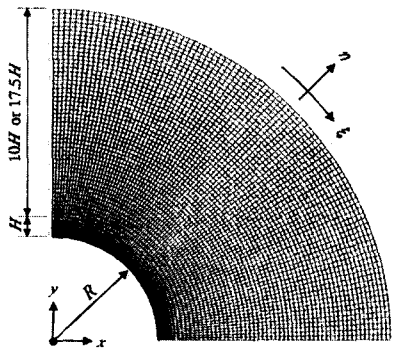

Fig.3 Computational grid

4. Results and Discussion

Figure 4 shows typical schlieren pictures of supersonic Coanda wall jets for R/H=6.0. These experiments were made for both the increase and decrease processes of the operating pressure ratio (p_0/p_a). For p_0/p_a=2.0 the Coanda jet flows along the curved surface due to the Prandtl-Meyer expansion waves appearing at the exit of the converging nozzle. With an increase in p_0/p_a, the Coanda wall jet detaches the curved wall surface but reattaches downstream of the separation point, forming a separation bubble on the curved wall. Shock wave forms at the separation point and the jet flow appears highly turbulent due to the interaction of the shock wave with shear layers (see p_0/p_a=2.9). With a further increase in p_0/p_a, the jet fully detaches the curved wall surface, showing a typical supersonic free jet. A multiple of shock waves appear in the jet, leading to the repeated expansion and compression regions. The jet shows a periodic cell structure, as seen in the supersonic free jet.

For the decrease of p_0/p_a, the Coanda jet is quite different from that observed in the increase of p_0/p_a. Unlike the jet flow field for p_0/p_a=2.0 of the increase process of the operating pressure ratio, the jet fully detaches the curved wall and is similar to the flow field seen in

p_0/p_a=2.9. This is due to entrainment effects of the ambient air flow induced by the supersonic jet. For the further decrease of p_0/p_a, the jet attaches the curved wall surface again. A hysterisis phenomenon is found in the two processes of the increase and decrease of the operating pressure ratio. For the increase process of p_0/p_a, the jet detachment is due to the shock wave/boundary layer interactions on the curved wall surface. However for the decrease process of p_0/p_a, the operating pressure ratio necessary to reattach the jet result from the tendency of the fully detached jet to keep its momentum flow toward the jet axis direction. In this case the entrainment effects of the ambient air can not be relatively significant compared with this tendency. In the present experiment, the similar hysterisis phenomenon was also found for different R/H values. As a consequence, it may be reasonable to characterize the supersonic Coanda jet flow field by several distinct patterns. Depending on the operating pressure ratio, the supersonic Coanda jet is typically classified into three different flow fields, such as the fully attached flow (type-A), the attached flow with a separation bubble (type-B), and the fully detached flow (type-C). The three flow patterns of supersonic Coanda jet mentioned above are also confirmed from the static wall pressures, which were measured along the curved wall surface.

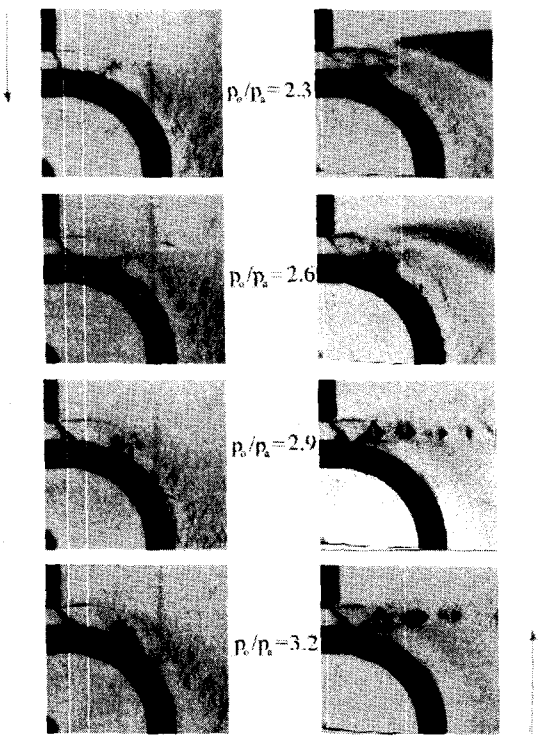

(a) Increase of p_o/p_a (b) Decrease of p_o/p_a

Fig.4 Schlieren pictures (R = 60 mm, H = 10 mm)

Figure 5 shows the static pressure distributions along the curved wall surfaces with R/H=5.0and 6.0(H=10mm). The abscissa is the angle α of the measuring point, as shown in Fig.2, and on the ordinate is the local pressure p represented in nondimensional form divided by the initial total pressure p_0.

For the Type-A of a fully attached flow, the static pressures rapidly decreases at the vicinity of the nozzle exit before fluctuating due to the repeated compression and expansion waves in the jet, and then approaches the atmospheric pressure level. In this case two experimental data for R/H=5.0 and 6.0 shows qualitatively similar feature.

For type-B of the attached flow with a local separation bubble, the separation region for R/H=5.0 (po/pa=2.7) covers the region from α=30 to 48 deg. For R/H=6.0 it extends the region from α=25 to 60 deg, leading to more extensive separation bubble, compared with the case of R/H=5.0. These regions are indicated by A and B in the figure, respectively.

For type-C of the fully detached flow, the static pressure distributions are quite different from those of type-A and type-B, as mentioned above. The static pressures for the two cases of R/H=5.0 and 6.0 drop at the vicinity of the nozzle exit but then remain unchanged up to far downstream field. The constant pressure is essentially the same to the atmospheric pressure.

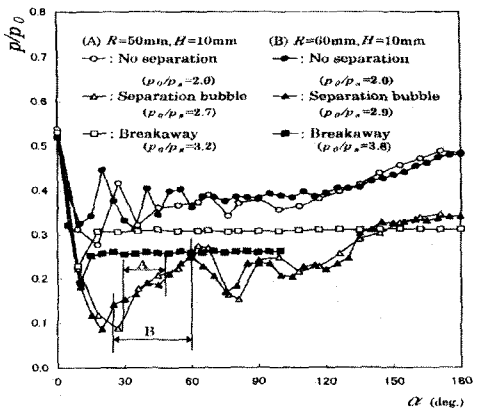

Fig.5 Static pressure distributions along Coanda surface

Figure 6 represents the experimental data to characterize the flow attachment and detachment of Coanda jet on the curved wall. The operating pressure ratio p_0/p_a and the height of the convergent nozzle exit were changed for a given curved wall surface with R=60mm. Symbols of open and closed circles denote the experimental data of the increase and decrease processes of the pressure ratio, respectively. The detachment and attachment of Coanda jet indicate some hysterical change for two processes of

the operating pressure ratio. As seen from the figure the hysterisis loop becomes small with an increase in H, equivalent to a decrease in R/H. Both the being jet momentum for detachment and the entrainment effect of ambient air toward the curved surface for attachment seem to affect the hysterisis loop.

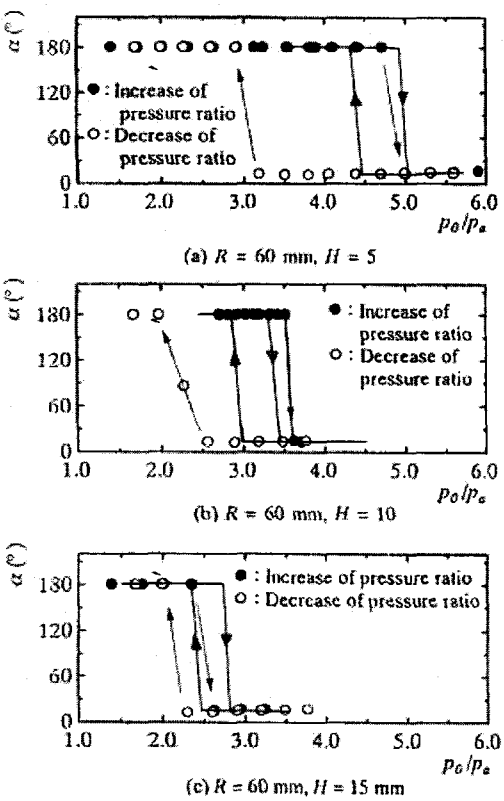

Fig.6 Hysterical characteristics of Coanda jet

It is also found that the operating pressure ratio necessary to detach and attach the jet increases with R/H. This is explained by the fact that the jet momentum is proportional to H. A higher value of H leads to a larger mass flow rate issuing from the converging nozzle. The jet of smaller momentum would be more sensitive to the etrainment effects of the ambient air, consequently leading to a higher operating pressure ratio necessary to detach the jet with an increase in R/H. The unsteady Euler computations were performed to predict this kind of hysterical phenomenon. This was mainly due to the limited computer capability used in the present work. A comparison can still be made from both experimental and numerical results. The present computations predict the jet detachment with a reasonable accuracy, but fail to predict the jet attachment. The full unsteady Navier-Stokes computations may improve this disagreement. Here it should, however, be noted that the hysterical phenomenon for both the increase and decrease processes of the operating pressure ratio can also be found in computations, which show a strong influence of R/H on the hysterical loop.

In Figure 8, the predicted and experimented static pressures along the curved wall are compared for two-cases of R/H=5.0 and 6.0. Three different turbulence models were used for the purpose of comparison.

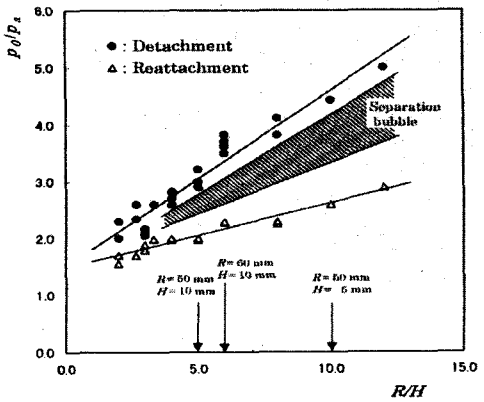

Fig.7 Effect of R/H and p_0/p_a on detachment and reattachment of Coanda jet

It is found that for type-A of a fully attached flow, the present Nevier-Stokes computations predict the experimental pressures with a reasonable accuracy, but the agreement is not good for type-B with a large separation bubble.

Turbulence model used to predict the supersonic Coanda jet flow may in part be responsible for the disagreement. The full 3-dimensional computations may improve the numerical prediction. Further work is needed to predict the hysterical phenomenon of the supersonic Coanda jet flow.

5. Conclusions

Experimental and computational studies were carried out in order to clarify the effects of pressure ratios and nozzle configurations on the flow characteristics of the supersonic Coanda jet. The results obtained are summarized as follows :

(1) The supersonic Coanda wall jet has three distinct features, depending on the operating pressure ratio and R/H. These are the fully attached flow (type-A), the attached flow with a separation bubble (type-B), and the fully detached flow (type-C).

(2) The values of p_0/p_a for detachment and reattachment of the Coanda jet increase almost lineally with an increase of R/H. This results in an increase of hysteresis loop.

(3) The hysterical phenomenon for the jet detach-

ment and reattachment exists for both the increase and decrease process of the operating pressure ratio. The hystrical loop becomes larger with R/H.

(4) Euler computation predict the jet detachment but it fails to predict the jet reattachment.

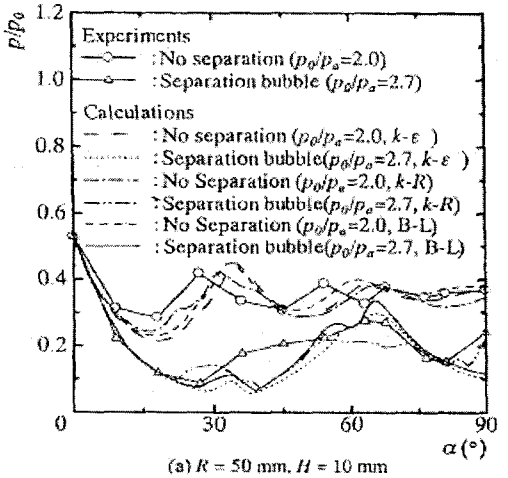

(a) R = 50 mm, H = 10 mm

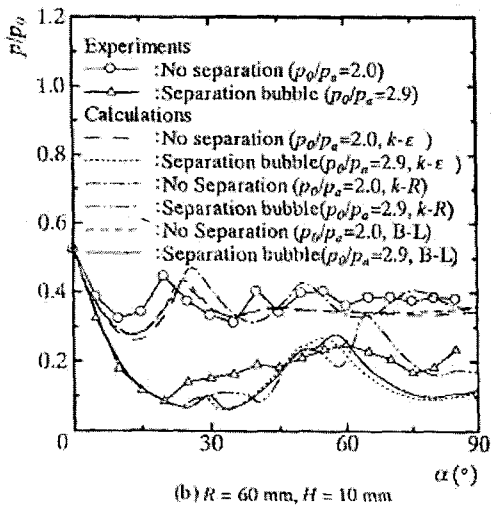

(b) R = 60 mm, H = 10 mm

Fig.8 Predicted and experimented static pres -sure along Coanda surface

References

(1) Cornelius, K. C. and Lucius, G. A., 1994, "Physics of Coanda Jet Detachment at High-Pressure Ratio," *Jour of Aircraft*, Vol.31, No.3, pp.591-596.

(2) Gregory-Smith, D. G. and Gilchrist, A. R. 1987, "The Compressible Coanda Wall Jet an Experi mental Study of Jet Structure and Breakaway," *Journal of Heat and Fluid Flow*, Vol.8, pp.156- 164.

(3) Shrewsbury, G. D., 1989, "Numerical Study of a Research Circulation Control Airfoil Using Navier-Stokes Methods," *Journal of Aircraft*, Vol.26, No.1, pp.29-34.

(4) Williams, S.L. and Franke, M.E., 1992, "Navier-Stokes Methods to Predict Circulation Control Airfoil Performance," *Journal of Aircraft*, Vol.29, No.2, pp.243-249.

(5) Linton, S. W., 1994, "Computation of the Post stall Behavior of a Circulation Controlled Air foil," *Journal of Aircraft*, Vol.31, No.6, pp.1273- 1280.

(6) Wilkins, J., Witheridge, R.E., Densty, D.H., Ma son, J. T. M. and Newby, N., 1977, "The Design, Development and Performance of Indair and Mar-dair Flares," *Offshore Technology Conference*, 2822, pp.123-130.

(7) Desty, D. H., 1983, "No Smoke with Fire," *Proc Instn Mech Engrs*, 197A, pp.159-170.

(8) Sawada, K. and Asami, K., 1997, "Numerical Study on Underexpanded Coanda Jet," *Journal of Aircraft*, Vol.34, No.5, pp.641-647.

(9) Bevilaqua, P. M. and Lee, John D., 1969, "Design of Supersonic Coanda Jet Nozzles," *AIAA* Paper 84-0333.

(10) Sridhar, I. and Tu, P.K.C., 1969, "Experimental Investigation of Curvature Effects on Turbulent Wall Jets," *Aero Journal of RAS* Vol. 73, pp.977.

(11) Bradshaw, P., 1974, "Effects of Streamline Cur vature on Turbulent Flow," *AGARD-AG*-169.

(12) Kim, H.D.et al.,2000, "Experimental and Nu merical Studies of Supersonic Coanda Wall Jet, "AIAA paper 2000-0814